229 (2023) 212170

Contents lists available at ScienceDirect

Geoenergy Science and Engineering

journal homepage: www.sciencedirect.com/journal/geoenergy-science-and-engineering

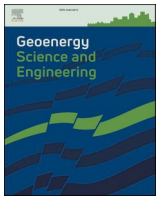

Alterations in wettability and immiscible fluid flows by bacterial biosurfactant production for microbial enhanced oil recovery: Pore-scale micromodel study

Taehyung Park [a,1,*], Tae-Hyuk Kwon [a], Sheng Dai [b]

[a] Department of Civil and Environmental Engineering, Korea Advanced Institute of Science and Technology (KAIST), Daejeon, South Korea
[b] School of Civil and Environmental Engineering, Georgia Institute of Technology, GA, United States

ARTICLE INFO

Keywords:
Micromodel
Biosurfactant
Wettability
Enhanced oil recovery
Pore-scale observation
Emulsification
Demulsification

ABSTRACT

This study investigates alterations in wettability during bacterial growth and biosurfactant production and its ensuing impacts on immiscible fluid flow at a pore scale. Here, pore-scale experiments were carried out with two types of patterned micromodels. First, the experiments with a single-channel micromodel visually captured the real-time wettability alteration from oil-wet to water-wet while cultivating the model bacteria *Bacillus subtilis*, in which the bacterial cells and produced biosurfactant significantly lowered the contact angles, including static, advancing, and receding angles, by ~70–90°. In addition, the emulsification-demulsification phenomena at brine-oil interfaces and the contact angle alterations by biofilms were also observed. Second, the surfactant-flooding process was emulated in the experiments with multi-channel micromodel while examining the effect of surfactant concentration on oil sweeping efficiency. The results of the multi-channel micromodel experiment show that a biosurfactant concentration of 70 mg/L, which is twice the critical micelle concentration, resulted in a lower contact angle, reduced residual oil saturation, and more homogeneous and stable patterns of oil displacement. Particularly, a significant level of variations in the contact angles at fluid-solid interfaces was observed in the multi-channel micromodel, and the extent of variation decreased with an increase in biosurfactant concentration. The presented results provide insights into pore-scale coupled microbial-hydrological processes in porous media as well as the biosurfactant-aided flooding in microbial enhanced oil recovery (MEOR).

1. Introduction

Wettability, the fluid's affinity to its host porous medium, has a pronounced effect on the fluid displacement patterns in porous media (Kathel and Mohanty, 2013; Wang et al., 2011; Zhang et al., 2006a). Therefore, the wettability among oil, brine and rock-forming minerals plays a critical role in determining the oil recovery efficiencies, particularly when implementing enhanced oil recovery (EOR) from a nearly depleted hydrocarbon reservoir (Kathel and Mohanty, 2013; Morrow, 1990; Seethepalli et al., 2004; Zhang et al., 2006a,2006b). Most oil reservoirs are oil-wet or mixed-wet due to long-term exposure to oil (Kathel and Mohanty, 2013; Seethepalli et al., 2004). Injection of fluids containing surface-active agents, mostly surfactants, is generally applied in EOR practices, which alters the rock wettability into water-wet, induces spontaneous imbibition of injecting fluids, and consequently improves the oil mobility in hydrocarbon reservoirs (Liang et al., 2021; Wu et al., 2008).

Meanwhile, biosurfactants are proposed as an effective alternative to synthetic surfactants, due to their intrinsically innocuous and biodegradable nature (Desai and Banat, 1997; Ron and Rosenberg, 2001). Several biosurfactants are reported to have more or less the same capability as the synthetic chemical surfactants in altering interfacial properties, *e.g.*, lipopeptides (*i.e.*, surfactin and pumilacidin) (Jacques, 2011) and glycolipids (i.e., rhamnolipids, sophorolipids and trehalolipids) (Benincasa et al., 2004; Daverey and Pakshirajan, 2010; White et al., 2013). Amongst, surfactin produced by bacteria *Bacillus subtilis* strains has proved its efficiency in reducing the oil-brine interfacial tension (IFT, γ) and the wettability of oil, brine, and rock minerals from

* Corresponding author.
E-mail addresses: taehyung.park@austin.utexas.edu (T. Park), t.kwon@kaist.ac.kr (T.-H. Kwon), sheng.dai@ce.gatech.edu (S. Dai).
[1] Current affiliation: McKetta Department of Chemical Engineering, University of Texas at Austin, Austin, TX, United States

https://doi.org/10.1016/j.geoen.2023.212170
Received 18 April 2022; Received in revised form 12 June 2023; Accepted 18 July 2023
Available online 19 July 2023

an intermediate water-wet ($\theta = \sim 45-50^{\circ}$) to a strong water-wet condition ($\theta = \sim 20-25^{\circ}$) (Park et al., 2019). It has been reported that such a reduced capillary factor ($\gamma \cdot \cos\theta$) improves the sweeping efficiencies of oil in a porous medium and results in oil recovery enhancement (Kim and Santamarina, 2014; Park et al., 2017, 2019). However, these previous studies were limited to a batch-type of experiments or numerical modeling of flow behaviors in porous media, and there has been no reported attempt to measure wettability alteration caused by biosurfactant production in porous media, while culturing bacteria *in situ* and examining the effect on immiscible fluid flow behaviors.

The water flooding for EOR causes oil-brine interfaces in motion, rather than in an immobile state. Therefore, dynamic contact angles gain more relevance than static contact angle (Jafari and Jung, 2017). Dynamic contact angles refer to the contact angles of which three-phase contact line is in motion on the surface. Dynamic contact angles are categorized as the advancing angle and the receding angle; the advancing contact angle is the angle generated in the course of a wetting process, and the receding angle is generated during a dewetting process (Jiang et al., 1979; Johnson et al., 1977). There have been a few attempts to use the micro-focus X-ray computed tomography (micro-CT) for capturing the wettability alteration during flooding of low-salinity water and nanofluids (Ali et al., 2021; Chen et al., 2020; Lebedeva and Fogden, 2011) and measuring the static contact angles with rocks and sand packs (Andrew et al., 2014; Scanziani et al., 2017). However, is difficult to measure the dynamic contact angles using the micro-CT and image fluids in a motion due to the slow imaging process (Jafari and Jung, 2017; Khishvand et al., 2016). Moreover, exposure to X-ray sources is by nature lethal to living cells (Lehnert and Moroson, 1971; Luo et al., 2013). On the other hand, optically transparent microfluidic devices are widely used to visualize and understand the pore-scale habits of multiphase fluids flows and *in situ* emergent phenomena (Beebe et al., 2002; Fan et al., 2018; Gogoi and Gogoi, 2019; Gravesen et al., 1993; Lifton, 2016; Mohammadi and Mahani, 2020; Saadat et al., 2020; Saadat et al., 2021; Seo et al., 2018; Squires and Quake, 2005; van Rooijen et al., 2022). Saadat et al. (2021) investigated the oil displacement during surfactant flooding by the effect of wettability alteration. They measured contact angles with and without the surfactant named Span 80 in a water-wet and oil-wet uniform micromodels. A study of Seo et al. (2018) is one of the few experimental studies that evaluated a biosurfactant in a micromodel, in which the oil-water IFT was measured in the presence of a nonionic biosurfactant, and effect of the biosurfactant on oil recovery rate was assessed through surfactin flooding tests. In addition, van Rooijen et al. (2022) measured the advancing and receding contact angles of H_2-water-glass in a micromodel to provide insights for underground hydrogen storage. Their parametric experimental study demonstrated dynamic contact angle decrement with increased channel widths and suggested that in a micromodel with 50 μm width provided most reliable contact angle measurements. However, the emergent process in porous media which couples bacterial growth, *in situ* biosurfactant production, their attachment at oil-water interfaces, and ensuing wettability modification remains poorly identified. Technical difficulty in visualizing oil-water interfaces in porous media with living micro-organisms hampers unveiling such microbial wettability modification.

Therefore, this study investigates the wettability modification by bacterial growth and biosurfactant production at a pore scale and its ensuing effect on fluid displacement behavior, which elucidates the key microbial EOR mechanisms. First, the model organism *B. subtilis* strain (ATCC21332) was cultured in single channel micromodel to observe evolutions of static and dynamic contact angles as well as emulsification at brine-oil interfaces during the bacterial cell growth and biofilm and biosurfactant production. This single-channel micromodel experiment examines the extent of modification in wettability by the bacterial biosurfactant production and whether or not the produced quantity would be sufficient to change the wettability to the biosurfactant's limit, as in the critical micelle concentration (CMC) condition. Second, the surfactant-flooding experiments were conducted in porous micromodel (multi-channel micromodel) to investigate pore-scale immiscible fluid displacement mechanisms in association with biosurfactant, while examining effect of surfactant concentration on oil sweeping efficiencies and contact angle hysteresis. Discussion on impact of biosurfactant-aided waterflooding follows.

2. Materials and methods

2.1. Micromodel fabrication

a. Single-Channel Micromodel

A single-channel micromodel (SCM) was designed to monitor the real-time transition of wettability during production of biosurfactants. A T-junction where two channels with the width of 50 μm and the aperture height of 100 μm (w × h) intersect is patterned in the single-channel micromodel, as shown in Fig. 1a and b. This T-junction facilitates droplet formation, and allows observation on the oil-brine interfaces and measurement of the contact angles. Furthermore, a serpentine section before the T-junction is placed in each channel as a fluid resistor (Fig. 1b), and this provides better control of fluid flows and more reliable measurement of advancing and receding contact angles when the fluids moved (Keller et al., 2007; Šikalo et al., 2005). Measuring dynamic contact angles in natural porous media is challenging because the capillary pressure unavoidably changes while displacing a fluid-fluid interface due to the irregular pore morphology (Måløy et al., 1992). Accordingly, the micromodel with a single-channel is suitable for dynamic contact angle measurement.

The single-channel micromodel was fabricated by a general soft photolithography process using polydimethylsiloxane (PDMS, Sylgard 184, Dow Corning, USA; (Hassanpourfard et al., 2014; Jang et al., 2019; Jang et al., 2017). In this study, both the top and bottom layers were fabricated with PDMS to ensure that all the wetted surfaces had the same physicochemical characteristics. The SU-8 master mold (MicroFIT, Korea) for the PDMS model was first made, a PDMS prepolymer solution was cured on the master mold at 85 °C for 2 h, and then the cured PDMS layer was carefully detached from the mold. The thickness of this top PDMS layer was 2.5 mm. Two inlets and one outlet for the 1/16-inch tubing installation were made with a circular punch. The bottom PDMS layer with the thickness of 2.5 mm was produced on the top of a slide glass (75 × 26 × 1 mm). Thereafter, the top PDMS layer was placed and attached on the bottom PDMS layer. The fabricated single-channel micromodel was autoclaved and dried before use.

b. Multi-Channel Micromodel

The effect of biosurfactant concentration on oil displacement rate in porous media was evaluated with a multi-channel micromodel with the width of 7.1 mm and the length of 3.6 mm, as shown in Fig. 1c. The model housed total of 780 uniform-sized cylindrical pillars, each 150 μm in diameter. The aperture height was 150 μm. The center-to-center distance between two neighboring pillars was 180 μm. The total pore volume of the micromodel was 0.71 mm^3. Similar to the single-channel micromodel, two layers of PDMS, of which the thickness was 5 mm each, were attached on top of a slide glass. The preparation of the multi-channel micromodel, including inlet and outlet installation, followed the same procedure with the single-channel micromodel (Fig. 1d).

2.2. Model bacterium selection and inoculum preparation

This study used *Bacillus subtilis* strain ATCC 21332 (acquired from the American Type Culture Collection, ATCC) as the model microorganism. The *Bacillus* spp. Genus is omnipresent in subsurface and aquatic environments and can survive under harsh environments such as extreme pH, high salinity (Simpson et al., 2011), high temperature, and high

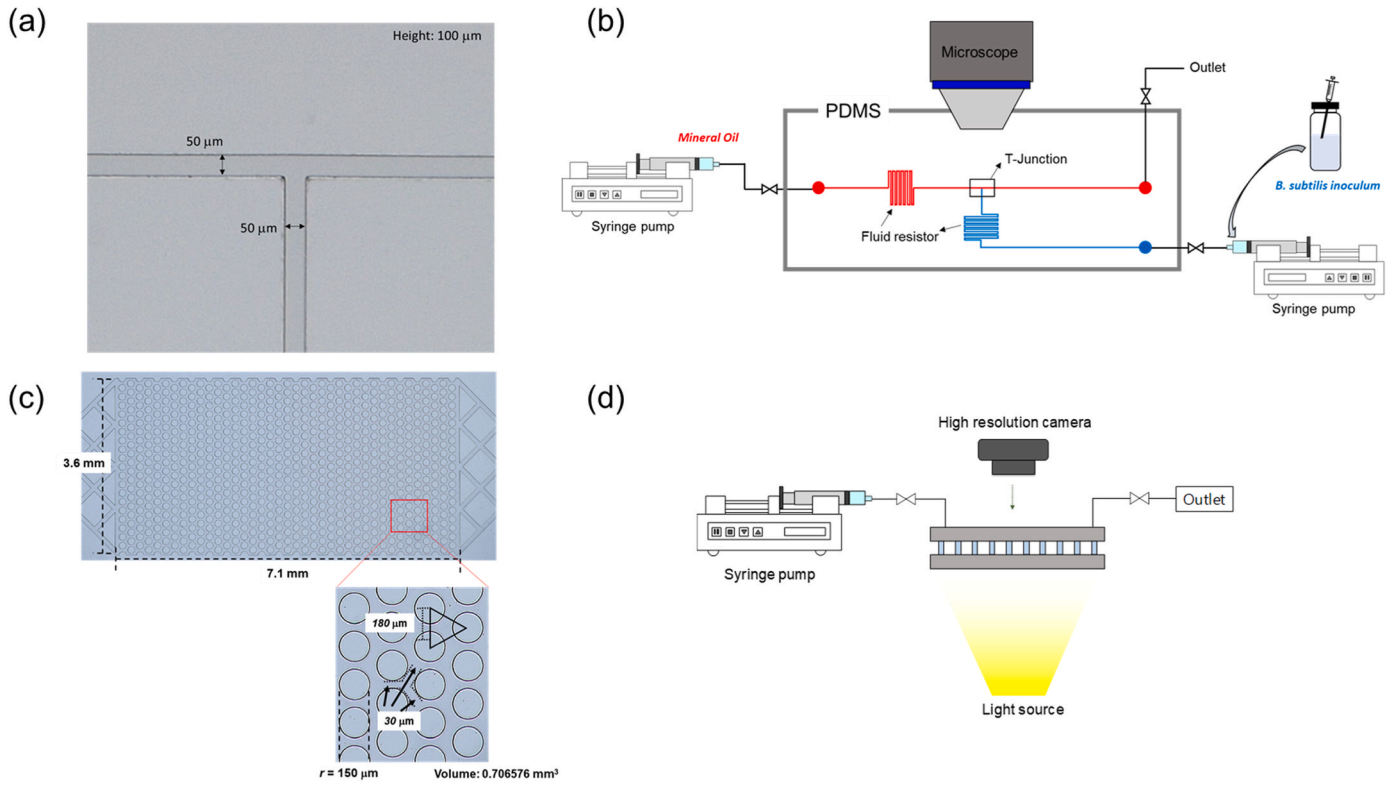

Fig. 1. Schematic descriptions of the geometries of (a) the single-channel micromodel, (b) the multi-channel micromodel, and their corresponding experimental setups for (c) the single-channel and (d) the multi-channel micromodels.

pressure (Yakimov et al., 1995). Accordingly, *Bacillus* spp. Have been popularly investigated as the model organism for evaluating the feasibility of MEOR application (Al-Bahry et al., 2013; Al-Wahaibi et al., 2014; Park et al., 2017; Peet et al., 2015). Their ability to form endospores supports high survivability when subjected to elevated temperature, desiccation, or chemical disinfectants (Nicholson et al., 2000). More importantly, *Bacillus* spp. Have been frequently found in oil reservoirs (Datta et al., 2018; Korenblum et al., 2005; Simpson et al., 2011), and hence this study presumes that the *Bacillus* strain be an ideal model microorganism to explore the effect of bacterial activities and bio-products on MEOR.

The mineral salt medium was used as a culture medium, as listed in Table 1 (Park et al., 2017). The mineral salt medium contained adequate amounts of carbon (glucose), nitrogen (nitrate and ammonium) and trace elements (manganese, potassium, and iron, etc.), and this composition was optimized for surfactin production, as suggested in the previous studies (Cooper and Goldenberg, 1987; Rangarajan and Clarke, 2016; Shaligram and Singhal, 2010; Wei and Chu, 2002; Wei et al., 2007). This mineral salt medium was filter-sterilized with a 0.2 μm sterile syringe filter (Chmlab Group, Terrassa-Barcelona, Barcelona, Spain) prior to use.

Table 1
Medium composition for *Bacillus subtilis* growth and surfactin production.

Compound	Concentration
Carbon source	
Glucose	40 g/L
Mineral salt medium	
$MgSO_4$	8.0×10^{-4} M
$CaCl_2$	8.0×10^{-4} M
$FeSO_4$	8.0×10^{-4} M
Na_2EDTA	8.0×10^{-4} M
$MnSO_4$	8.0×10^{-4} M
Nitrogen source	
NH_4Cl	0.1 M
$NaNO_3$	0.118 M
Phosphate buffer	
KH_2PO_4	0.03 M
Na_2HPO_4	0.04 M

The starter culture was prepared by the cultivation in the nutrient broth (Difco, BD, NJ, United States) at 37 °C. From the starter culture, 1%v/v of a freshly grown aerobic culture was transferred to the mineral salt medium. The culture was then incubated for 48 h at 37 °C with no shaking. The single-channel micromodel tests used brine (i.e., mineral salt medium) containing *B. subtilis* culture at 1%v/v as the inoculum for *in situ* cultivation in the model. Meanwhile, surfactin solutions were injected into oil-filled multi-channel micromodels, which examined the oil displacement rate by the surfactant flooding. The surfactin solutions were prepared by dissolving the purified surfactin in a fresh medium while varying the dissolved surfactin concentrations. The CMC of surfactin produced by *B. subtilis* is approximately 34 μmol/L, which is equivalent to ~35 mg/L (Park et al., 2019). Therefore, 0, 10.5, 17.5, 35, and 70 mg/L of surfactin solutions were prepared, which represented 0 ×, 0.3 ×, 0.5 ×, 1 ×, and 2 × CMC, respectively.

Meanwhile, pure surfactin was extracted and prepared using the acid precipitation method (Fig. S1 in Supporting Information). The Fourier Transform-infrared Spectroscopy (FT-IR) qualitatively confirmed the class of the extracted biosurfactant as surfactin, as shown in Fig. S1b. The functional groups of the extracted biosurfactant were compared with those of the standard surfactin sample acquired from Sigma-Aldrich (Sigma Aldrich, MO, United States). The details of biosurfactant extraction procedures are available in the authors' previous literature (Park et al., 2017).

2.3. Experimental procedure and data reduction

a. Wettability Observation with the Single-channel Micromodel

The transition of oil-brine wettability on PDMS surfaces during growth of biosurfactant-producing bacteria was evaluated using the single-channel micromodel. During the tests, experiments with the micromodel were performed under an optical microscope (DM 500 B, Leica, Wetzlar, Germany). The microscopic images were taken every 5 min for 150 h and with the 2, 4, 10×, and 50× objective lenses. In addition, videos were occasionally taken to measure the advancing/receding contact angles. Alkane hydrocarbons were not appropriate to be used in the PDMS-based micromodel experiments because they cause swelling of PDMS (Dangla et al., 2010). Instead, mineral oil, which had the viscosity of 15 cP, was used as the oil phase in this study. Mineral oil used in this study is composed of saturated and aromatic hydrocarbons, and *B. subtilis* is one of the hydrocarbon-degrading bacteria. It should be noted that the ability of *B. subtilis* to degrade aromatic compounds can enhance the production yield of biosurfactant in the presence of oil (Ghribi and Ellouze-Chaabouni, 2011; Martínez-Checa et al., 2007).

Before the tests, all the wetting parts including the PDMS micromodel, tubes and valves were autoclaved. The micromodel was firstly filled with the mineral oil; and the brine containing *B. subtilis* culture was then injected into the oil-filled micromodel at a flow rate of 1 μL/min. During the brine injection, the oil injection was halted. The micromodel was equipped with two inlet ports for the injection of mineral oil and the *B. subtilis* inoculum (Fig. 1b). The mineral oil was dyed with Sudan III (0.1 wt%) for better visual distinction between the oil and the brine phases. The chosen flow rate produced a laminar flow with the Reynold number R_e of 0.22. For injection, we used a syringe pump (NE-1002X; New Era Systems Inc., NY, USA) with a Norm-ject 5 mL Luer lock syringe. Both fluids inevitably passed the fluid resistor intervals for flow velocity control. The T-junction structure facilitated two immiscible fluids in contact each other and created the menisci of oil and brine, which enabled monitoring of the contact angle of the oil-brine-PDMS system.

Throughout microbial growth and biosurfactant production, time-lapsed images of the immiscible mixed fluids (oil and brine) were acquired for ~150 h. The static contact angles were measured when the flow was halted and the fluid-fluid interfaces sat motionless. The dynamic advancing and receding contact angles were measured by pushing and retracting respectively the brine phase using the brine injection pump. Considering that the flow velocity affects the dynamic contact angle, the injection flow rate was fixed at 1 μL/min and the internal flow velocity of the fluids was kept at less than 50 μm/s for reliable and consistent estimates. The static and dynamic contact angles of oil-brine-PDMS in the acquired images were determined using ImageJ software, by drawing a straight line tangent to the fluid meniscus and the other line coincident with the flat PDMS surface (Stalder et al., 2006). In addition, the presence of bacterial biomasses such as bacterial cells and bacterial biofilms also affects fluid transport. Local accumulation of biomasses with *B. subtilis* appeared in the flow channels of the single-channel micromodel, and this rendered flow velocity variations during advancing and receding of interfaces, which hampered reliable estimation of moving velocity of the oil-brine interfaces. Therefore, it is worth pointing out that we determined the dynamic contact angles only when oil-brine interfaces were located in a clear channel with no microbial substances, such that there was no obstacle when the fluids advanced or receded.

b. Surfactant Flooding Test with the Oil-filled Multi-channel Micromodel

The surfactant flooding tests were carried out in the multi-channel micromodel to evaluate the role of biosurfactants in decreasing the residual oil saturation and increasing the oil displacement efficiency in porous media. As graphically depicted in Fig. 1d, the top-view images of the micromodel were acquired with a high-resolution camera (Canon EOS 100D, Tokyo, Japan) equipped with a macro lens (Canon 100 mm 2.8f, Tokyo, Japan). Mineral oil was used as an oil phase, and it pre-saturated the multi-channel micromodel to mimic a typical drainage process during EOR practice. The flooding fluid (or invading fluid) was the surfactin solution, the mixtures of the cell-free brine and purified surfactin at the surfactin concentrations of 0, 10.5, 17.5, 35 and 70 mg/L. The flooding fluid was dyed with methylene blue (0.3 wt%) for the better visual distinction between the oil and the brine phases. The surfactin solutions were filter-sterilized with a 0.2 μm filter to remove any biomass or residual substances for better visibility in the micromodel.

The surfactant flooding test procedure followed the typical tertiary recovery process that extracts the remnant oil from an oil reservoir with the thermal, gas and chemical treatments (Lake, 1989). The water flooding first displaces the oil in the porous medium, and the surfactant flooding follows which further sweeps residual oil. In our tests, the empty clean micromodel was initially saturated with the mineral oil. The brine injection was then conducted at a flow rate of 0.5 μL/min (Reynold's number $R_e = 0.004$) with a syringe pump (NE-1002X; New Era Systems Inc., NY, USA). This brine injection continued for 2 h, which was equivalent to 113 pore volumes. Upon this 2 h-long brine injection, the oil saturation in the micromodel was leveled off, and reached a stationary residual state. Thereafter, the surfactin solution was injected at the same flow rate for additional 2 h.

The pore saturation of the oil was calculated by analyzing the acquired time-lapsed images of the mutli-channel micromodel after the surfactant flooding. Further, the static contact angles were determined by the Tangent method, which measures the contact angle at the crossing point of the three phases oil, brine and PDMS (Chau, 2009; Rotenberg et al., 1983). The oil-brine-PDMS contact angle in each case was measured at least 74 locations and the variations in the contact angles were analyzed and fitted to the normal distribution.

3. Results and discussion

3.1. Observations from single-channel micromodel

3.1.1. In-situ biosurfactant production and wettability modification

Wettability, the affinity of an immiscible fluid to a specific solid surface, determines the capillary pressure between two immiscible fluids and affects the immiscible fluid flows in porous media; the contact angles are directly related to the wettability. The static contact angle is referred to as the contact angle measured when the contacting interface of two immiscible fluid phases has no motion. Whereas the dynamic contact angles are quantified when the interface is in motion on a solid rock surface by either receding or advancing. This section presents the temporal changes in static and dynamic contact angles measured during the growth of biosurfactant-producing bacteria in the single-channel micromodel.

Fig. 2a shows the variations in mineral oil-brine-PDMS contact angles over the course of *B. subtilis* cultivation. Owing to the cell growth and biosurfactant production, the static contact angle decreased from ~110 to 115° to ~35−41° over 144 h, as shown in Fig. 2b. The advancing contact angle decreased from ~138 to 151° to ~48−60°, whereas the receding contact angle decreased from ~90 to 102° to ~16−30°. It is confirmed that biosurfactant generation and accumulation caused gradual reductions in the contact angles, which indicates that the PDMS surface was initially oil-wet, and became more water-wet by *B. subtilis*.

The contact angles began to decrease when 5–10 h elapsed since the start of the cultivation. All the contact angles were leveled off and converged to the lower limits after approximately 30 h. The reduction trends appeared to be consistent between static and dynamic angles. The convergence to lower limits indicates the surfactin concentration in brine reached the CMC at ~30 h. Previous studies have reported that 30−40 mg/L of surfactin concentration is required to reduce the contact angle to the lower limit, in other words, CMC (Abdel-Mawgoud et al., 2008; Davis et al., 1999; Liu et al., 2015; Park et al., 2019). Accordingly, our test result suggests that cultivation of *B. subtilis* with the mineral salt

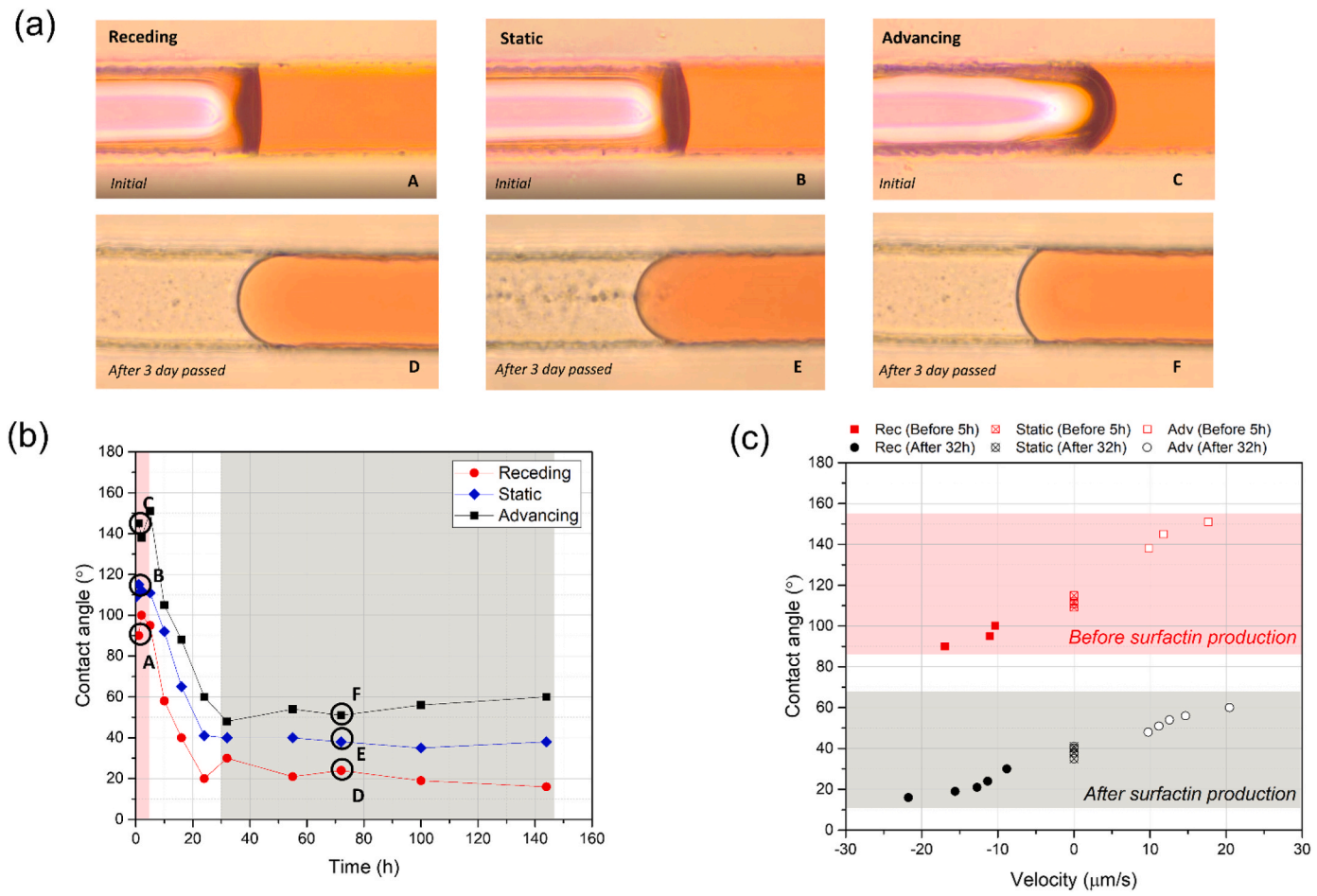

Fig. 2. (a) Snapshots of examples of receding (A, D), static (B, E), and advancing (C, F) contact angles before and after the bacterial cultivation. (b) The dynamic and static contact angle evolutions with time. And (c) the contact angle variations by velocity. Note: Negative velocity on the x-axis indicates the pump retracted the water phase for receding contact angle measurement, and where the positive velocity indicates when the pump pushed the fluid for advancing contact angle measurement. Zero velocity is when the fluid was standstill after the pump is paused.

medium produced a sufficient amount of surfactin, 30–40 mg/L at minimum, and altered the wettability to the maximum level.

Meanwhile, the difference in advancing and receding contact angles is defined as the contact angle hysteresis, and it indicates activation energy required for the movement of a droplet on a surface. The contact angle hysteresis is attributable to the heterogeneities in pore structure, surface roughness and chemical interaction between fluids and rock surface (Behnoudfar et al., 2022; Johnson et al., 1977; Juanes et al., 2006). Expectedly, the contact angle hysteresis has an impact on the residual and capillary trapping of oil in a reservoir (Juanes et al., 2006). Our results show that the contact angle hysteresis (the advancing angle minus the receding angle) differed before and after bacterial cultivation, as shown in Fig. 2b. The contact angle hysteresis was ~48° at the start of the cultivation, but it soon decreased to less than ~32° when 24 h elapsed. This indicates that bacterial cell growth and biosurfactant production in a brine phase can facilitate immiscible fluid displacement by lowering the contact angle hysteresis and the activation energy required for fluid mobility.

Also, our results have an implication to selection of a proper one among the static, receding, and advancing contact angles to better predict the fluids' behavior in porous media. The dynamic contact angles are more suitable for predicting the immiscible fluid flows as the menisci of immiscible fluids are in motion together. The advancing contact angle, the upper boundary of the contact angle, can be used to predict the invasion and injectability of a non-wetting fluid, water in water flooding cases, based on the capillary pressure using the Young-Laplace equation (Jafari and Jung, 2017; Young, 1805). Whereas, the receding contact angle, the lower boundary of the contact angle, can be used to determine the capillary pressure and mobility of a wetting phase, oil in water flooding EOR practices.

3.1.2. *Effects of fluid velocity in measured dynamic contact angles*

The dynamic contact angles are widely used to describe wetting, spreading, and adhesion processes between a liquid and a solid (Keller et al., 2007; Šikalo et al., 2005). Earlier observations have shown that the dynamic contact angle is dependent on various measurement parameters, including the drag (viscous and capillary) forces and the surface physical/chemical heterogeneity (Cassie and Baxter, 1944; Jiang et al., 1979; Johnson et al., 1977; Keller et al., 2007). Expectedly, the fluid velocity determines the drag force, and hence significantly affects the dynamic contact angle (Keller et al., 2007; Šikalo et al., 2005). This section explores the impact of flow velocity on the dynamic contact angles.

In this study, the oil-brine interface moved as a push-pull piston, and therefore, the flow velocity was identical to the moving velocity of the interface (Fig. 2a). Thereby, the fluid velocity was estimated using the video acquired for the dynamic contact angle measurement. Particularly, we chose two time intervals. The first time frame was the first 5 h, in which we assumed that the biosurfactant production was yet negligible and had no or minimal impact on the contact angles (denoted as Points A, B and C in Fig. 2b). The second time frame was the range after 32 h, where the contact angle converged to the lower limit value

(denoted as Points D, E and F in Fig. 2b). Meanwhile, the interval between 5 and 32 h was excluded, where the bacteria grew exponentially and produced the surfactin at a significantly rapid rate, such that this phase allowed insufficient time for the push and pull manipulation.

Fig. 2c shows the variations in the contact angles with the flow velocity. The velocity of 0 μm/s indicates the static contact angle with no fluid mobility. The positive velocity represents the advancing contact angle during pushing, and the negative velocity for the receding contact angle during retraction, respectively. The greater contact angle hysteresis was observed at the higher velocity. Before surfactin production, the advancing contact angle increased from ~110 to 115° at 0 μm/s, ~140° at 10 μm/s (by 24%), and to ~151° at 18 μm/s (by 34%). After surfactin production, the advancing contact angle increased from ~35 to 41° at 0 μm/s, ~~48° at 10 μm/s (by 26%), and to ~60° at 21 μm/s (by 58%). The receding angles also showed the same tendency.

Our results clearly show that the role of advancing/receding velocities in determining dynamic contact angles. The contact angle varied with the velocity when the velocity was less than 20 μm/s, and the advancing and receding contact angles were leveled off at the velocity greater than ~20–30 μm/s (Fig. 2c). This is fairly consistent with the previous study result which has reported that the contact angle becomes insensitive to advancing and receding velocity above 150–200 μm/s (Keller et al., 2007). Meanwhile, it is challenging to identify the range of flow velocity during water flooding practices in a hydrocarbon reservoir, because the fluid is presumed to flow radially from a well, such that the velocity decreases as it flows further away from the injection well. In addition, preferential flow path development as well as porosity and pore size of the formation rocks have profound effects on the flow velocity. Nevertheless, it has been reported that in a sandstone reservoir, the typical velocity of water advancement during waterflooding is in the order of 1 ft/day, equivalent to ~3.5 μm/s (Masalmeh, 2013). Therefore, the examined flow velocity range (0–20 μm/s) in this study is expected to cover the flow velocity observed in typical sandstone reservoirs and down to tight reservoirs with low permeability.

Nevertheless, it noted that the degree of contact angle modification was similar and consistent before and after surfactin production, regardless of flow velocity (Fig. 2c). The surfactin production by *B. subtilis* caused consistent reductions in contact angles by ~70–90° when receding, static, and advancing. This indicates that the efficacy of the produced surfactin in altering wettability from oil-wet to water-wet is valid, hardly affected by the movement of oil-brine interfaces.

3.1.3. Pore-scale observation of microbial cell growth

The single-channel micromodel test allowed the monitoring of bacterial cell growth, biofilm production, and cell attachments at a pore scale. Fig. 3 presents pore-scale observation of the bacterial growth during the cultivation of biosurfactant-producing bacteria, *B. subtilis*, in a defined medium inside the single-channel micromodel. When 16 h elapsed, the bacterial cell growth initiated. Thereafter, bacterial cells showed an exponential growth phase when 16–30 h elapsed, which is consistent with the optical density measured at 600 nm (Fig. 3b). After 40 h, bacterial cells started to form biofilms, the complex structures of microbiome in which bacterial cells are locally agglomerated with extracellular polymeric substances (EPS). The cell density in biofilms increased with time, which is commonly observed in nature (from 41 to 55 h elapsed in Fig. 3a). Overall, the cell growth rate observed in the single-channel micromodel agreed well with the batch culture experiment with the optical density measurement.

Fig. 4 revealed the effect of the bacterial cell presence on the static contact angle. This image was acquired in the no flux condition at 80 h elapsed when the concentration of surfactin reached the CMC. Note that at the CMC, the static contact angle was lowered to 35–41° (Fig. 2b). This was also seen in the oil-brine-PDMS contact angle in the cell-free region, as denoted in Fig. 4. By contrast, the contact angle of oil-brine-PDMS near the accumulated bacterial cells and biofilms was evidently higher (~60°) than that of the cell-free region (~35–36°). This clearly demonstrates that local accumulation of bacterial cells and biofilms increases the nearby contact angle and changes the neighboring surface wettability to be more oil-wet. Such effect is apparently limited to the

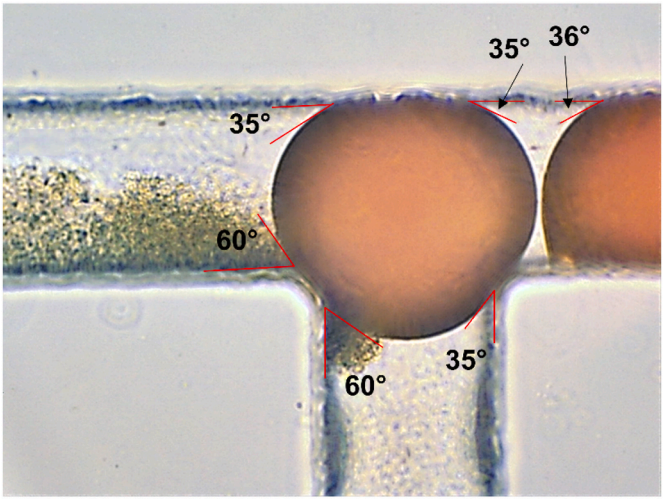

Fig. 4. Uneven contact angles at the immiscible oil-brine interfaces depend on bacterial biofilm accumulations. Note: The snapshot was taken at the static condition.

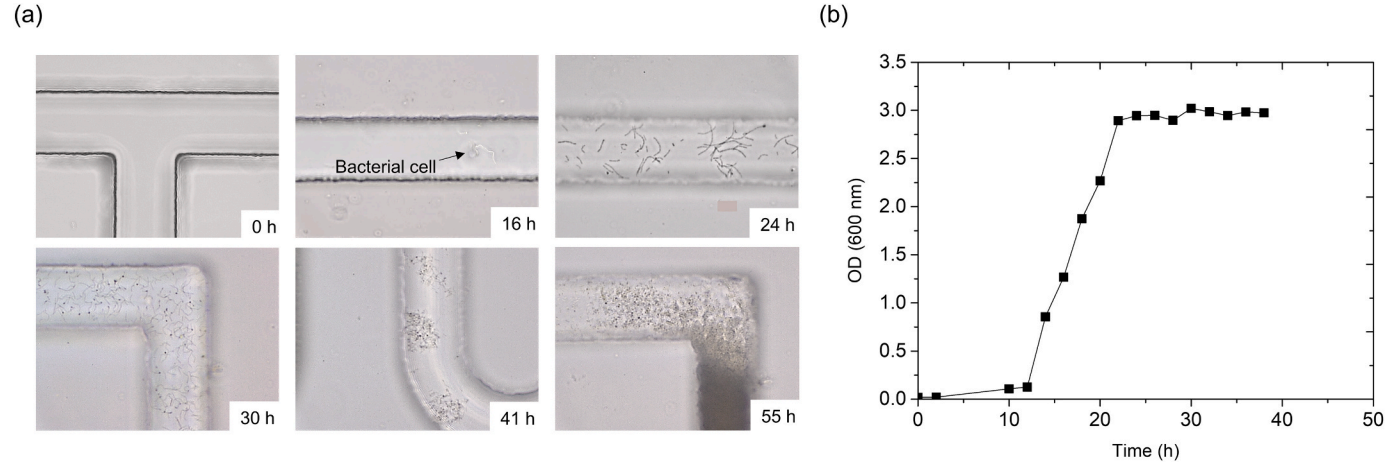

Fig. 3. Observations of (a) bacterial growth, biofilm accumulations and (b) optical density measured from a separate batch experiment.

case where the cells and biofilms are present in the immediate vicinity of the oil-brine-PDMS interfaces. Nonetheless, this observation implies that the accumulation of biomasses can alter the surface wettability and affect the immiscible fluid flow in a porous medium.

Our micromodel also suggests that use of micromodels allows real-time monitoring of bacterial cell growth, biofilm production, and cell attachments at a pore scale and it enables efficient and continuous quantification of bacterial growth without discarding samples, which can be a significant asset in microbiology studies, as no additional steps such as fluorescence staining or attaching a bead for density measurements are needed (Kim et al., 2019).

3.1.4. *Demulsification of oil-brine during biosurfactant accumulation*

An emulsion is defined as the dispersion of a liquid in another immiscible liquid. In the petroleum industry, the formation of a crude oil emulsion is ineluctable owing to several sources of mixing, including flow through porous rocks, bottom hole perforations, and presence of emulsifiers, such as asphaltenes or chemical additives (Abdulredha et al., 2020; Liu et al., 2020). Because separating the water in oil emulsion needs an additional refining process, the emulsion in the petroleum industry is undesirable, but at the same time, unavoidable. Therefore, it is critical to understand the formation mechanism of oil emulsions as well as the demulsification process of oil emulsions in porous media.

The surfactant production facilitates emulsification of oil and water with the aid of mixing of immiscible oil and water during the cyclic flow. Fig. 5 captures the process of micro-scale oil-in-water emulsion. In the first stage (Fig. 5a), water and oil are immiscible with a clear meniscus. As bacteria soon grow and the surfactant is produced with time, the system changes to the bicontinuous microemulsion phase (Fig. 5b), where the micelles become swollen and are no longer spherical (Acosta et al., 2003). This bicontinuous microemulsion phase contains an approximately equal volume fraction of the oil and water phases, and two phases are interdispersed within the phase. Thereafter, the oil begins to break down into small microemulsions (Fig. 5c). Finally, the droplet size of the emulsion decreases to the nano-scale, as shown in Fig. 5d. Surfactant is not only a well-known surface-active agent, but also an emulsifier that lowers the surface tension between two immiscible liquids and stabilizes emulsions. Hydrophilic and hydrophobic parts of surfactant molecules promote absorption of surfactants at the interface between oil and water; thereby the surfactant molecules coat immiscible fluid droplets as emulsions and prevent them from coalescing.

Contrary to that, we also observed that the produced surfactin functioned as a demulsifier to break emulsions. To illustrate this, Fig. 6 displays time-lapsed snapshots of one location within the single-channel micromodel during an experiment when 123–125 h passed. In the beginning, there are monodisperse oil droplets with an initial diameter of ~40 μm in the channel. Over time, these small emulsion droplets collide and coalesce to a larger single droplet having ~50 μm. This collision is facilitated by the arbitrary movements of droplets (Krebs et al., 2012). This demulsification is possibly attributable to the lowered pH as the pH regulates the activity of surfactin. This occurred after 5 days of experimental periods when the phosphate buffer was all consumed. The pH of the fresh medium was 6.8; with bacterial cultivation, it was lowered to 4.5 at the end of the experiment. It is known that surfactin loses its ability as a surface-active agent in low pH environments. Surfactin readily precipitates under an acidic condition due to the protonation of a carboxyl group (Abdel-Mawgoud et al., 2008; Park et al., 2020). It is presumed that the lowered pH in our system

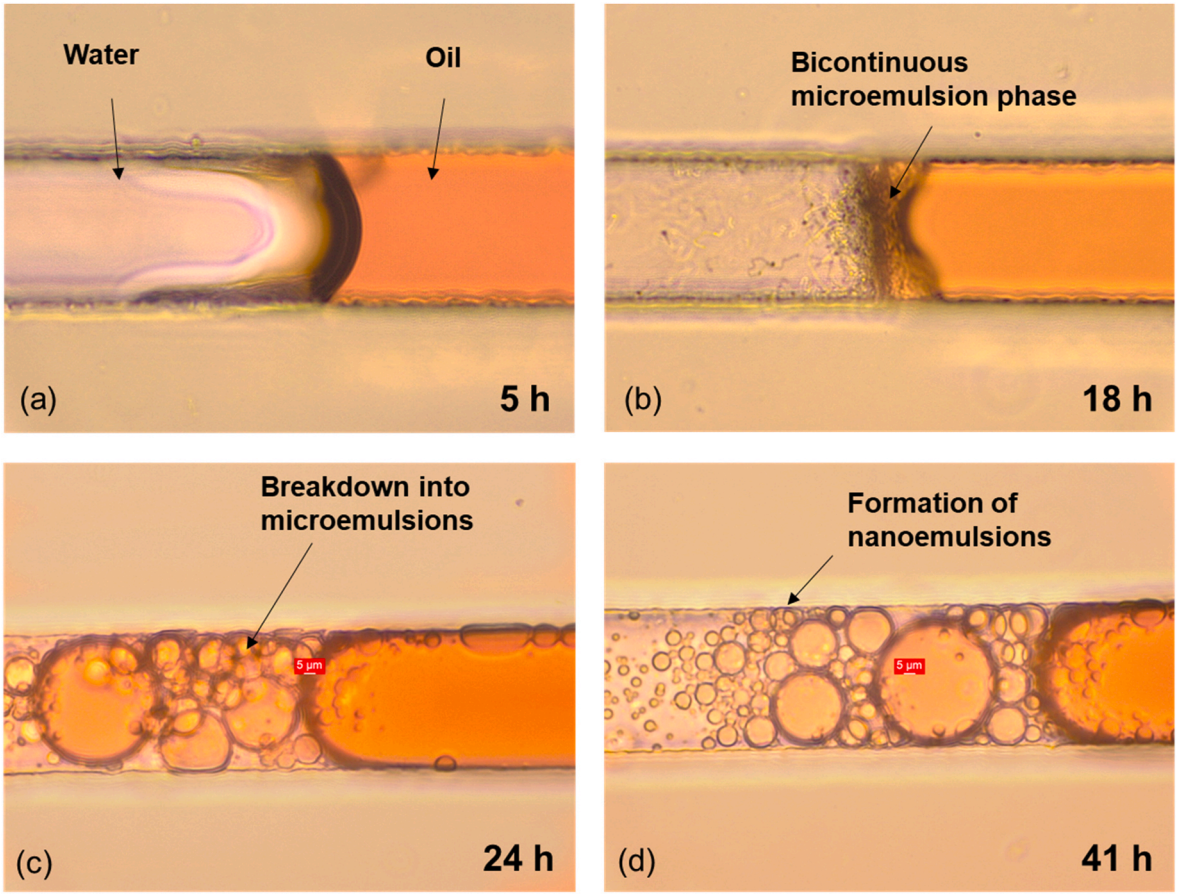

Fig. 5. Typical emulsification process from water/oil describing (a) before the emulsion is initiated, (b) bicontinuous microemulsion phase, (c) breakdown of oil into the microemulsions, and (d) the formation of nanoemulsions.

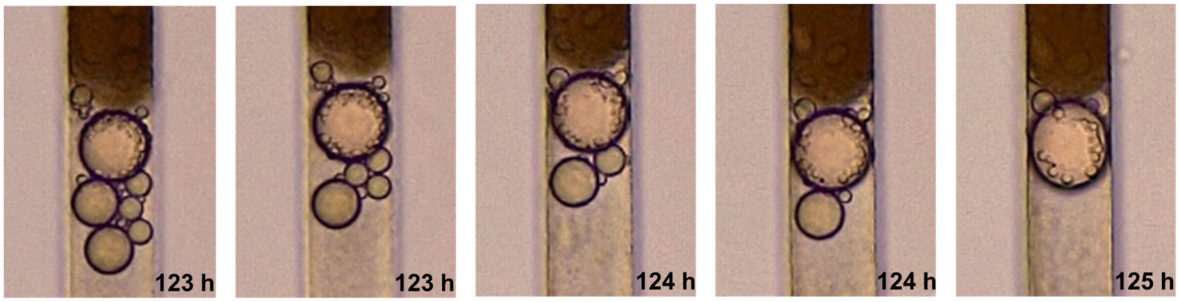

Fig. 6. Demulsification process as time passes. Collision and coalesce of oil droplets in water (oil-in-water emulsions) as time passes. Note that the width of the channel is 50 μm.

incapacitated the surfactin possibly with precipitation, and induced demulsification of emulsified droplets. This result is consistent with previous studies (Long et al., 2017; Sana et al., 2021; Yang et al., 2020), where they regulated pH to control the emulsification and demulsification of oil/water/surfactin systems. Our results also suggest a potential of controlling pH of injection water to selectively emulsify or separate oil and water during surfactin-aided water flooding practices.

3.2. Observations from the multi-channel microdel

3.2.1. Effects of biosurfactant on residual oil saturation

Residual oil saturations after surfactant flooding in the multi-channel micromodel were examined while varying the surfactin concentration for flooding. The water invasion into a mineral oil-filled porous micromodel was imposed with the mobility ratio of −1.5 and the capillary number of −5.1 for water flooding. The ensuing surfactant flooding was carried out with the mobility ratio of −1.9 and the capillary number of −5.0, respectively. The calculated mobility ratio and capillary number indicate that the invasion pattern of immiscible fluids was dominantly governed by capillary fingering in our porous micromodel (Cao et al., 2016; Lenormand et al., 1988).

Fig. 7 shows the oil displacement patterns of water flooding. For the first 2 h, water flooding with no additives proceeded. After 2 h of water flooding, biosurfactant-containing water was injected to simulate surfactant flooding and quantify enhancement of the displacement efficiency of oil in a porous medium. As mentioned earlier, 0, 10.5, 17.5, 35, and 70 mg/L of surfactin solutions were prepared, which represented 0 ×, 0.3 ×, 0.5 ×, 1 ×, and 2 × CMC, respectively. Prior to biosurfactant flooding, the water flooding yielded 82.9% of oil recovery while leaving the residual oil saturation of 17.1% within micromodel. Compartively, when flooding the surfactin-containing fluids at the surfactin concentration from 0.3 ×, 0.5 ×, 1 ×, and to 2 × CMC, the residual oil saturations gradually decreased to 11.7%, 9.2%, 1.9% and 0.3%, respectively. The result shows that the residual oil saturation decreases as the biosurfactant concentration in the flooding fluid increases. The lowered residual oil saturation and the greater oil displacement efficiency is attributable to the reduced IFT and the modified wettability in which the PDMS surface becomes more hydrophilic by surfactin. Interestingly, this positive effect of surfactin is noticeably effective even when the surfactin concentration is two times greater than CMC. In fact, the oil displacement is considerably improved when the surfactant concentration increases from 1 × CMC to 2 × CMC. This is possibly because the surface-active effect of surfactin is not uniform, but shows a wide distribution over the micromodel.

3.3. Biosurfactant-induced wettability modification

Fig. 8a shows the sub-sections within the multi-channel micromodels after either water flooding or surfactant flooding. These enlarged sections depict clear contrasts in the shapes of oil-water menisci between the cases with and without biosurfactant. We analyzed the contact angle at all the contacts and determined their distributions, as shown in

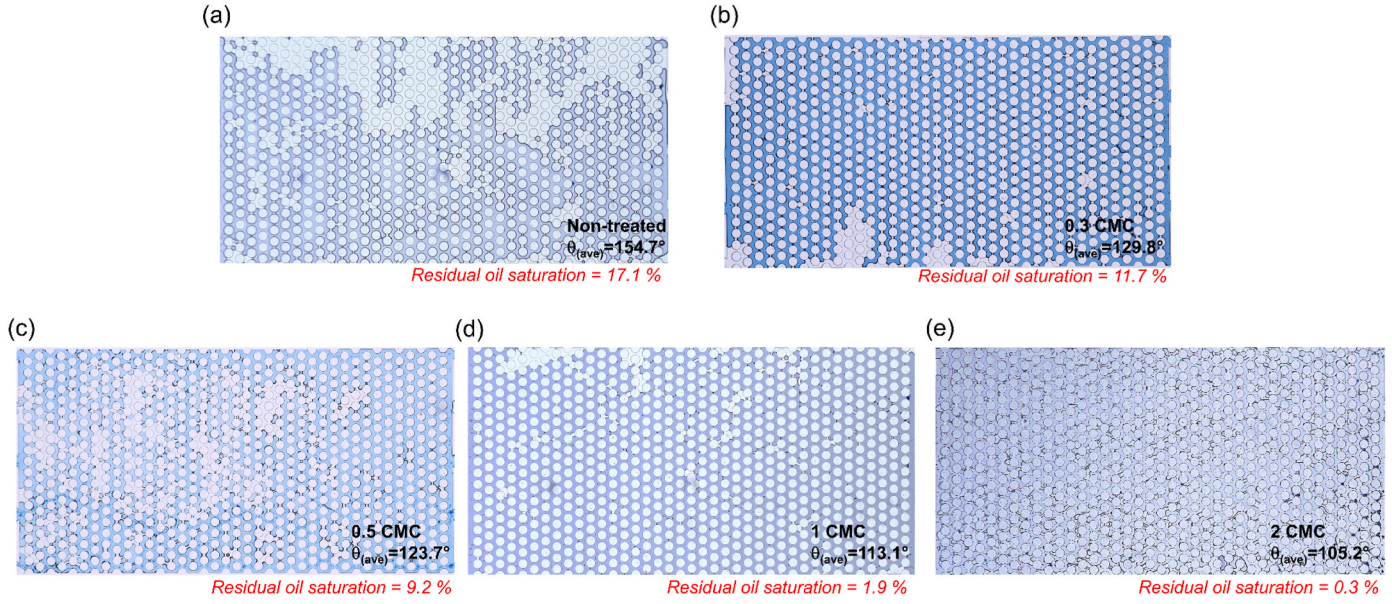

Fig. 7. Residual oil saturation changes in multi-channel micromodel (MCM) after 2 h biosurfactant flooding. The figures represent the final projections of (a) 0, (b) 0.3, (c) 0.5, (d) 1 and (e) 2 critical micelle concentration (where 1 critical micelle concentration is equivalent to 35 mg/L).

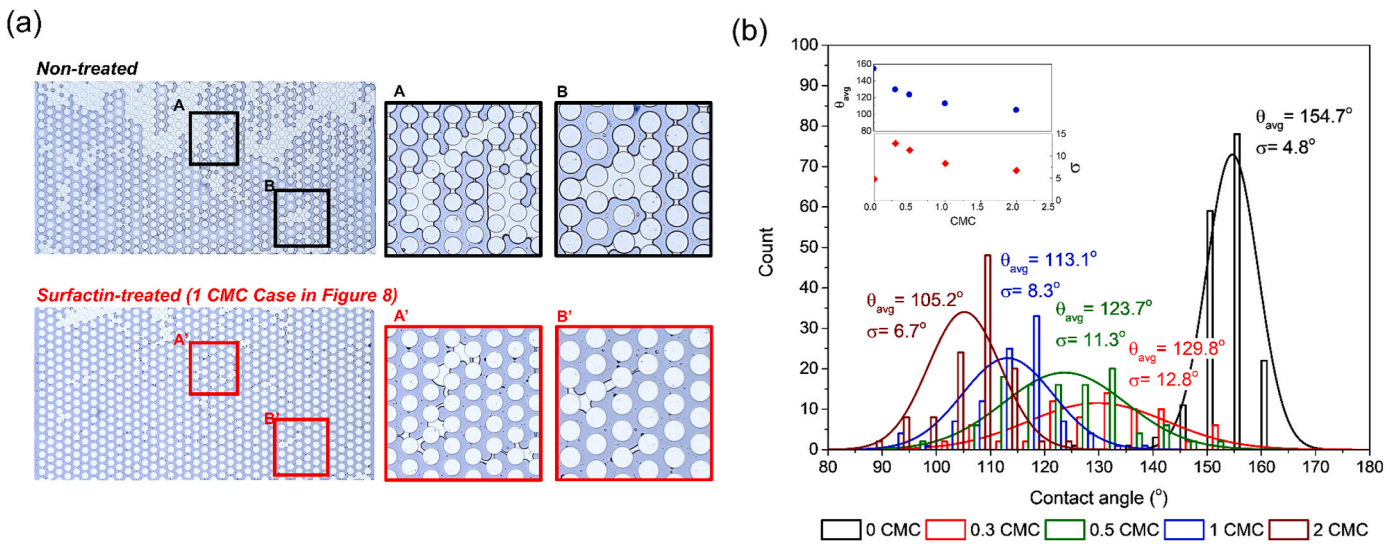

Fig. 8. (a) Contact angle comparison of non-treated and surfactin-treated micromodels and (b) distributions of contact angles of mineral oil-water-PDMS systems. Inset figures A and B and A′ and B′ show the oil-water interfaces before and after surfactin flooding. θavg represents the average contact angle, and σ indicates the standard deviation.

Fig. 8b. Expectedly, the average contact angles (θ_{avg}) decrease as the surfactin concentration increases. The average contact angle of the water-oil-PDMS interface θ_{avg} before surfactin treatment is 154.7°, and it decreases to 129.8° for 0.3 × CMC, 123.7° for 0.5 × CMC, and 113.1° when the surfactin solution at 1 × CMC (35 mg/L) is flooded (Fig. 8b). When the concentration of surfactin is doubled to 2 × CMC, the average contact angle θ_{avg} decreases to the lowest value of 105.2°. Therefore, together with the reduced oil-water IFT, those wettability modifications in the PDMS surface to be more water-wet contribute to the significant increase in the oil sweeping efficiency.

The standard deviation σ indicates the spatial variation in the contact angle observed in the multi-channel micromodel, and implies the heterogeneity in wetting behavior, such as surfactin adsorption or surfactin effectiveness. As the CMC increases from 0.3 × CMC to 2 × CMC, the standard deviation σ and hence the spatial variation decreases. This is consistent with the study by Mirchi et al. (2014), where they reported that the spatial variation in contact angle is generally suppressed with the presence of surfactant (Mirchi et al., 2014). This indicates that the surfactin adsorption and distribution become more homogeneous with an increase in the surfactin concentration of the flooding solution.

By contrast, it is worth pointing out that the contact angle distribution without biosurfactant shows the least variation with the lowest standard deviation σ of 4.8° among the tested cases. The cases with surfactin (0.3 × , 0.5 × , 1 × , and 2 × CMC) show the greater standard deviation and the wider variation in contact angle than the case without surfactin. This is due to the uneven distribution of surfactin driven by the surfactin flooding. First, before the system reaches the CMC, the surfactin monomers can be unevenly adsorbed in some local regions, and there are the other locations with insufficient amounts of surfactin. Particularly with 0.3 × CMC and 0.5 × CMC, before micelles are formed, there are some ranges on the right tails overlapping with the distribution of 0 × CMC. This possibly implies the absence of surfactin on those oil-water menisci. Furthermore, the larger variations in the contact angle with surfactin could also be attributable to the geometric effect associated with the reduced droplet size. The surfatin significantly reduces the oil droplet size, and thus the droplet's relative position to the PDMS pillars heavily affects the contact angle.

Our results suggest that the contact angle variation, or spatial heterogeneity in wettability, can greatly increase with surfactant flooding, and this becomes worse particularly when the surfactant concentration is less than the CMC. Note that such a high spatial variability in contact angle was observed in the controlled experiments with the micromodels which have a regular pore geometry with a uniform pore throat size and minimal chemical and physical heterogeneity. Whereas, natural porous media, such as formation rocks, in oil reservoirs can be highly heterogeneous. In specific, the mineral composition and pore fluid chemistry determine the electrical surface potential of the rock mineral surfaces, and hence those have a pronounced effect on the surfactant adsorption efficiency on the rock surfaces. Accordingly, loss of surfactant inevitably occurs during surfactant flooding due to unwanted and heterogeneous surfactant adsorption near wellbores. This class of surfactant transport problems still remains a challenge in EOR. On the other hand, another MEOR strategy could use the stimulation of bacterial biosurfactant production *in situ*. This would involve the inoculation of nutrients and stimulation of indigenous microorganisms to produce biosurfactants in place within a reservoir. As the nutrient solution would flow along the main fluid paths, the microbial growth will occur in the immediate vicinity where the nutrients are transported. As a result, to some extent biosurfactant production can be controlled to occur uniformly along the main fluid paths. This could be beneficial to avoid unwanted surfactant loss in near-wellbore regions and to achieve a wide spread of surfactant for uniform and effective transition of wettability in a far-field. Nonetheless, further research is warranted to identify spatial variation (heterogeneity) of surfactant adsorption in natural rocks and develop a novel way for effective surfactant transport to enhance oil recovery.

4. Conclusion

Wettability plays a vital role in the displacement of fluids in a porous medium. This study investigated the potential of using micromodels to understand wettability transitions during bacterial surfactant accumulation at the pore scale. With different types of micromodels, experiments were conducted to evaluate the biosurfactant-induced MEOR process by altering the wettability. A single-channel micromodel was fabricated to observe the biosurfactant-induced wettability modification in real-time. It enabled direct observations of bacterial growth and biofilm accumulations in a porous medium. Also, the time-lapse stages of dynamic-static contact angle changes and the emulsification/demulsification processes occurring at the water-oil interface were directly observed over the course of bacterial cultivations. With the single-channel micromodel, it was observed that both dynamic and static contact angles decrease as biosurfactant concentration increases over time. Also, dynamic contact angles varied owing to the internal velocity of fluids. Specifically, the receding contact angle decreased and the

advancing contact angle increased as the velocity increased. The multi-channel micromodel fabricated for the surfactant-flooding experiment was used to investigate wettability transitions with the addition of different concentrations of biosurfactants. The results showed that the imbibition rates and the residual oil saturation are directly related to the surfactant concentration, and the concentration of surfactant should be over CMC to achieve homogeneous wettability transition and high oil-sweeping performance.

Credit author statement

Taehyung Park: Conceptualization, Methodology, Validation, Formal analysis, Investigation, Writing – original draft, Writing – review & editing. Tae-Hyuk Kwon: Conceptualization, Methodology, Validation, Writing – review & editing, Resources, Supervision, Project administration, Funding acquisition. Sheng Dai: Supervision, Investigation, Writing – review & editing.

Declaration of competing interest

The authors declare the following financial interests/personal relationships which may be considered as potential competing interests: Taehyung Park, Tae-Hyuk Kwon, Sheng Dai reports financial support was provided by Korea Agency for Infrastructure Technology Advancement (KAIA).

Data availability

Data will be made available on request.

Acknowledgments

This work was supoorted by the National Research Foundation of Korea (NRF) grant funded by the Korea government (MSIT) (NRF-2022R1A4A5031447), and by the National Research Foundation of Korea (NRF) grant funded by the Korea government (MSIT) (No. NRF-2022R1A4A5031447).

Appendix A. Supplementary data

Supplementary data to this article can be found online at https://doi.org/10.1016/j.geoen.2023.212170.

References

Abdel-Mawgoud, A.M., Aboulwafa, M.M., Hassouna, N.A.-H., 2008. Characterization of surfactin produced by *Bacillus subtilis* isolate BS5. Appl. Biochem. Biotechnol. 150 (3), 289–303.
Abdulredha, M.M., Aslina, H.S., Luqman, C.A., 2020. Overview on petroleum emulsions, formation, influence and demulsification treatment techniques. Arab. J. Chem. 13 (1), 3403–3428.
Acosta, E., Szekeres, E., Sabatini, D.A., Harwell, J.H., 2003. Net-average curvature model for solubilization and supersolubilization in surfactant microemulsions. Langmuir 19 (1), 186–195.
Al-Bahry, S., et al., 2013. Biosurfactant production by *Bacillus subtilis* B20 using date molasses and its possible application in enhanced oil recovery. Int. Biodeterior. Biodegrad. 81, 141–146.
Al-Wahaibi, Y., et al., 2014. Biosurfactant production by *Bacillus subtilis* B30 and its application in enhancing oil recovery. Colloids Surf., B 114, 324–333.
Ali, H., et al., 2021. Experimental investigation and two-phase flow simulation of oil and nanofluids on micro CT images of sandstone for wettability alteration of the system. J. Pet. Sci. Eng. 204, 108665.
Andrew, M., Bijeljic, B., Blunt, M.J., 2014. Pore-scale contact angle measurements at reservoir conditions using X-ray microtomography. Adv. Water Resour. 68, 24–31.
Beebe, D.J., Mensing, G.A., Walker, G.M., 2002. Physics and applications of microfluidics in biology. Annu. Rev. Biomed. Eng. 4 (1), 261–286.
Behnoudfar, D., Dragila, M.I., Meisenheimer, D., Wildenschild, D., 2022. Contact angle hysteresis: a new paradigm? Adv. Water Resour. 161, 104138.
Benincasa, M., Abalos, A., Oliveira, I., Manresa, A., 2004. Chemical structure, surface properties and biological activities of the biosurfactant produced by *Pseudomonas aeruginosa* LBI from soapstock. Antonie Leeuwenhoek 85 (1), 1–8.
Cao, S.C., Bate, B., Hu, J.W., Jung, J., 2016. Engineering behavior and characteristics of water-soluble polymers: implication on soil remediation and enhanced oil recovery. Sustainability 8 (3), 205.
Cassie, A., Baxter, S., 1944. Wettability of porous surfaces. Trans. Faraday Soc. 40, 546–551.
Chau, T., 2009. A review of techniques for measurement of contact angles and their applicability on mineral surfaces. Miner. Eng. 22 (3), 213–219.
Chen, Y., et al., 2020. Geochemical controls on wettability alteration at pore-scale during low salinity water flooding in sandstone using X-ray micro computed tomography. Fuel 271, 117675.
Cooper, D.G., Goldenberg, B.G., 1987. Surface-active agents from two *Bacillus* species. Appl. Environ. Microbiol. 53 (2), 224–229.
Dangla, R., Gallaire, F., Baroud, C.N., 2010. Microchannel deformations due to solvent-induced PDMS swelling. Lab Chip 10 (21), 2972–2978.
Datta, P., Tiwari, P., Pandey, L.M., 2018. Isolation and characterization of biosurfactant producing and oil degrading *Bacillus subtilis* MG495086 from formation water of Assam oil reservoir and its suitability for enhanced oil recovery. Bioresour. Technol. 270, 439–448.
Daverey, A., Pakshirajan, K., 2010. Sophorolipids from *Candida bombicola* using mixed hydrophilic substrates: production, purification and characterization. Colloids Surf., B 79 (1), 246–253.
Davis, D., Lynch, H., Varley, J.J.E., Technology, M., 1999. The production of surfactin in batch culture by *Bacillus subtilis* ATCC 21332 is strongly influenced by the conditions of nitrogen metabolism. Enzym. Microb. Technol. 25 (3–5), 322–329.
Desai, J.D., Banat, I.M., 1997. Microbial production of surfactants and their commercial potential. Microbiol. Mol. Biol. Rev. 61 (1), 47–64.
Fan, Y., Gao, K., Chen, J., Li, W., Zhang, Y., 2018. Low-cost PMMA-based microfluidics for the visualization of enhanced oil recovery. Oil Gas Sci. Technol. 73, 26.
Ghribi, D., Ellouze-Chaabouni, S., 2011. Enhancement of *Bacillus subtilis* lipopeptide biosurfactants production through optimization of medium composition and adequate control of aeration. Biotechnol. Res. Int. 653654.
Gogoi, S., Gogoi, S.B., 2019. Review on microfluidic studies for EOR application. J. Pet. Explor. Prod. Technol. 9 (3), 2263–2277.
Gravesen, P., Branebjerg, J., Jensen, O.S., 1993. Microfluidics-a review. J. Micromech. Microeng. 3 (4), 168.
Hassanpourfard, M., et al., 2014. Protocol for biofilm streamer formation in a microfluidic device with micro-pillars. J. Vis. Exp. 90.
Jacques, P., 2011. Biosurfactants. Springer.
Jafari, M., Jung, J., 2017. Direct measurement of static and dynamic contact angles using a random micromodel considering geological CO_2 sequestration. Sustainability 9 (12), 2352.
Jang, H., et al., 2019. Traction microscopy with integrated microfluidics: responses of the multi-cellular island to gradients of HGF. Lab Chip 19 (9), 1579–1588.
Jang, H., et al., 2017. Homogenizing cellular tension by hepatocyte growth factor in expanding epithelial monolayer. Sci. Rep. 7 (1), 1–10.
Jiang, T.-S., Soo-Gun, O., Slattery, J.C., 1979. Correlation for dynamic contact angle. J. Colloid Interface Sci. 69 (1), 74–77.
Johnson Jr., R.E., Dettre, R.H., Brandreth, D.A., 1977. Dynamic contact angles and contact angle hysteresis. J. Colloid Interface Sci. 62 (2), 205–212.
Juanes, R., Spiteri, E., Orr Jr., F., Blunt, M., 2006. Impact of relative permeability hysteresis on geological CO_2 storage. Water Resour. Res. 42 (12).
Kathel, P., Mohanty, K.K., 2013. EOR in tight oil reservoirs through wettability alteration. In: SPE Annual Technical Conference and Exhibition. Society of Petroleum Engineers.
Keller, A., Broje, V., Setty, K., 2007. Effect of advancing velocity and fluid viscosity on the dynamic contact angle of petroleum hydrocarbons. J. Pet. Sci. Eng. 58 (1–2), 201–206.
Khishvand, M., Alizadeh, A., Piri, M., 2016. In-situ characterization of wettability and pore-scale displacements during two-and three-phase flow in natural porous media. Adv. Water Resour. 97, 279–298.
Kim, S., Lee, S., Kim, J.-K., Chung, H.J., Jeon, J.S., 2019. Microfluidic-based observation of local bacterial density under antimicrobial concentration gradient for rapid antibiotic susceptibility testing. Biomicrofluidics 13 (1), 014108.
Kim, S., Santamarina, J.C., 2014. Engineered CO_2 injection: the use of surfactants for enhanced sweep efficiency. Int. J. Greenh. Gas Control 20, 324–332.
Korenblum, E., et al., 2005. Production of antimicrobial substances by *Bacillus subtilis* LFE-1, *B. firmus* H2O-1 and *B. licheniformis* T6-5 isolated from an oil reservoir in Brazil. J. Appl. Microbiol. 98 (3), 667–675.
Krebs, T., Schroen, K., Boom, R., 2012. A microfluidic method to study demulsification kinetics. Lab Chip 12 (6), 1060–1070.
Lake, L.W., 1989. Enhanced Oil Recovery. Prentice Hall Inc.
Lebedeva, E.V., Fogden, A., 2011. Micro-CT and wettability analysis of oil recovery from sand packs and the effect of waterflood salinity and kaolinite. Energy Fuel. 25 (12), 5683–5694.
Lehnert, S., Moroson, H., 1971. X-ray-induced single-strand breaks in DNA of *E. coli* B/r: effect of irradiation and postirradiation conditions. Radiat. Res. 45 (2), 299–310.
Lenormand, R., Touboul, E., Zarcone, C., 1988. Numerical models and experiments on immiscible displacements in porous media. J. Fluid Mech. 189, 165–187.
Liang, T., et al., 2021. Surfactant-EOR in tight oil reservoirs: current status and a systematic surfactant screening method with field experiments. J. Pet. Sci. Eng. 196, 108097.
Lifton, V.A., 2016. Microfluidics: an enabling screening technology for enhanced oil recovery (EOR). Lab Chip 16 (10), 1777–1796.
Liu, Q., Lin, J., Wang, W., Huang, H., Li, S., 2015. Production of surfactin isoforms by *Bacillus subtilis* BS-37 and its applicability to enhanced oil recovery under laboratory conditions. Biochem. Eng. J. 93, 31–37.

Liu, Y., et al., 2020. A review on emulsification via microfluidic processes. Front. Chem. Sci. Eng. 14 (3), 350–364.
Long, X., He, N., He, Y., Jiang, J., Wu, T., 2017. Biosurfactant surfactin with pH-regulated emulsification activity for efficient oil separation when used as emulsifier. Bioresour. Technol. 241, 200–206.
Luo, Y., et al., 2013. Targeted nanoparticles for enhanced X-ray radiation killing of multidrug-resistant bacteria. Nanoscale 5 (2), 687–694.
Måløy, K.J., Furuberg, L., Feder, J., Jøssang, T., 1992. Dynamics of slow drainage in porous media. Phys. Rev. Lett. 68 (14), 2161.
Martínez-Checa, F., Toledo, F., El Mabrouki, K., Quesada, E., Calvo, C., 2007. Characteristics of bioemulsifier V2-7 synthesized in culture media added of hydrocarbons: chemical composition, emulsifying activity and rheological properties. Bioresour. Technol. 98 (16), 3130–3135.
Masalmeh, S., 2013. Determination of Waterflooding Residual Oil Saturation for Mixed to Oil-Wet Carbonate Reservoir and its Impact on EOR, SPE Reservoir Characterization and Simulation Conference and Exhibition.
Mirchi, V., Saraji, S., Goual, L., Piri, M., 2014. Dynamic interfacial tensions and contact angles of surfactant-in-brine/oil/shale systems: implications to enhanced oil recovery in shale oil reservoirs. SPE Improved Oil Recovery Symposium. Society of Petroleum Engineers.
Mohammadi, M., Mahani, H., 2020. Direct insights into the pore-scale mechanism of low-salinity waterflooding in carbonates using a novel calcite microfluidic chip. Fuel 260, 116374.
Morrow, N.R., 1990. Wettability and its effect on oil recovery. J. Petrol. Technol. 42 (12), 484.
Nicholson, W.L., Munakata, N., Horneck, G., Melosh, H.J., Setlow, P., 2000. Resistance of Bacillus endospores to extreme terrestrial and extraterrestrial environments. Microbiol. Mol. Biol. Rev. 64 (3), 548–572.
Park, T., Jeon, M.-K., Yoon, S., Lee, K.S., Kwon, T.-H., 2019. Modification of interfacial tension and wettability in oil-brine-quartz system by in situ bacterial biosurfactant production at reservoir conditions: implications to microbial enhanced oil recovery. Energy Fuel. 33 (6), 4909–4920.
Park, T., et al., 2017. Biosurfactant as an enhancer of geologic carbon storage: microbial modification of interfacial tension and contact angle in carbon dioxide/water/quartz systems. Front. Microbiol. 8, 1285.
Park, T., Yoon, S., Jung, J., Kwon, T.-H., 2020. Effect of fluid–rock interactions on in situ bacterial alteration of interfacial properties and wettability of CO_2–brine–mineral systems for geologic carbon storage. Environ. Sci. Technol. 54 (23), 15355–15365.
Peet, K.C., et al., 2015. Microbial growth under supercritical CO_2. Appl. Environ. Microbiol. 81 (8), 2881–2892.
Rangarajan, V., Clarke, K.G., 2016. Towards bacterial lipopeptide products for specific applications—a review of appropriate downstream processing schemes. Process Biochem. 51 (12), 2176–2185.
Ron, E.Z., Rosenberg, E., 2001. Natural roles of biosurfactants. Environ. Microbiol. 3 (4), 229–236.
Rotenberg, Y., Boruvka, L., Neumann, A., 1983. Determination of surface tension and contact angle from the shapes of axisymmetric fluid interfaces. J. Colloid Interface Sci. 93 (1), 169–183.
Saadat, M., Tsai, P.A., Ho, T.-H., Øye, G., Dudek, M., 2020. Development of a microfluidic method to study enhanced oil recovery by low salinity water flooding. ACS Omega 5 (28), 17521–17530.
Saadat, M., Yang, J., Dudek, M., Øye, G., Tsai, P.A., 2021. Microfluidic investigation of enhanced oil recovery: the effect of aqueous floods and network wettability. J. Pet. Sci. Eng. 203, 108647.
Sana, S., Sengupta, D., Datta, S., 2021. Application of Biosurfactant in the Formulation of Petrochemical Products Such as Demulsifying/emulsifying Agents, Green Sustainable Process for Chemical and Environmental Engineering and Science. Elsevier.
Scanziani, A., Singh, K., Blunt, M.J., Guadagnini, A., 2017. Automatic method for estimation of in situ effective contact angle from X-ray micro tomography images of two-phase flow in porous media. J. Colloid Interface Sci. 496, 51–59.
Seethepalli, A., Adibhatla, B., Mohanty, K., 2004. Wettability alteration during surfactant flooding of carbonate reservoirs. In: SPE/DOE Symposium on Improved Oil Recovery. Society of Petroleum Engineers.
Seo, S., et al., 2018. Performance evaluation of environmentally benign nonionic biosurfactant for enhanced oil recovery. Fuel 234, 48–55.
Shaligram, N.S., Singhal, R.S., 2010. Surfactin–a review on biosynthesis, fermentation, purification and applications. Food Technol. Biotechnol. 48 (2), 119–134.
Šikalo, Š., Wilhelm, H.-D., Roisman, I., Jakirlić, S., Tropea, C., 2005. Dynamic contact angle of spreading droplets: experiments and simulations. Phys. Fluids 17 (6), 062103.
Simpson, D.R., Natraj, N.R., McInerney, M.J., Duncan, K.E., 2011. Biosurfactant-producing *Bacillus* are present in produced brines from Oklahoma oil reservoirs with a wide range of salinities. Appl. Microbiol. Biotechnol. 91 (4), 1083.
Squires, T.M., Quake, S.R., 2005. Microfluidics: fluid physics at the nanoliter scale. Rev. Mod. Phys. 77 (3), 977.
Stalder, A.F., Kulik, G., Sage, D., Barbieri, L., Hoffmann, P., 2006. A snake-based approach to accurate determination of both contact points and contact angles. Colloids Surf. A Physicochem. Eng. Asp. 286 (1–3), 92–103.
Wang, Y., et al., 2011. Surfactant induced reservoir wettability alteration: recent theoretical and experimental advances in enhanced oil recovery. Petrol. Sci. 8 (4), 463–476.
Wei, Y.-H., Chu, I.-M., 2002. Mn^{2+} improves surfactin production by *Bacillus subtilis*. Biotechnol. Lett. 24 (6), 479–482.
Wei, Y.-H., Lai, C.-C., Chang, J.-S., 2007. Using Taguchi experimental design methods to optimize trace element composition for enhanced surfactin production by *Bacillus subtilis* ATCC 21332. Process Biochem. 42 (1), 40–45.
White, D., Hird, L., Ali, S., 2013. Production and characterization of a trehalolipid biosurfactant produced by the novel marine bacterium *Rhodococcus* sp., strain PML026. J. Appl. Microbiol. 115 (3), 744–755.
Wu, Y., Shuler, P.J., Blanco, M., Tang, Y., Goddard, W.A., 2008. An experimental study of wetting behavior and surfactant EOR in carbonates with model compounds. SPE J. 13 (1), 26–34.
Yakimov, M.M., Timmis, K.N., Wray, V., Fredrickson, H.L., 1995. Characterization of a new lipopeptide surfactant produced by thermotolerant and halotolerant subsurface *Bacillus licheniformis* BAS50. Appl. Environ. Microbiol. 61 (5), 1706–1713.
Yang, Z., et al., 2020. Application of biosurfactant surfactin as a pH-switchable biodemulsifier for efficient oil recovery from waste crude oil. Chemosphere 240, 124946.
Young, T., 1805. An essay on the cohesion of fluids. Philos. Trans. R. Soc. 95, 65–87.
Zhang, D.L., Liu, S., Puerto, M., Miller, C.A., Hirasaki, G.J., 2006a. Wettability alteration and spontaneous imbibition in oil-wet carbonate formations. J. Pet. Sci. Eng. 52 (1–4), 213–226.
Zhang, P., Tweheyo, M.T., Austad, T., 2006b. Wettability alteration and improved oil recovery in chalk: the effect of calcium in the presence of sulfate. Energy Fuel. 20 (5), 2056–2062.